Lagrangian structure functions in turbulence: A quantitative comparison between experiment and direct numerical simulation

L. Biferale,[1] E. Bodenschatz,[2,a)] M. Cencini,[3] A. S. Lanotte,[4,a)] N. T. Ouellette,[5,b)] F. Toschi,[6] and H. Xu[5]

[1]*International Collaboration for Turbulence Research and Dipartimento Fisica and INFN, Università di "Tor Vergata," Via della Ricerca Scientifica 1, 00133 Roma, Italy*
[2]*International Collaboration for Turbulence Research, Max Planck Institute for Dynamics and Self-Organization, Am Fassberg 17, D-37077 Goettingen, Germany and Laboratory of Atomic and Solid-State Physics, Cornell University, Ithaca, New York 14853, USA*
[3]*International Collaboration for Turbulence Research, INFM-CNR, SMC Dipartimento di Fisica, Università di Roma "La Sapienza," p.zle A. Moro 2, 00185 Roma, Italy and Istituto dei Sistemi Complessi-CNR, via dei Taurini 19, 00185 Roma, Italy*
[4]*International Collaboration for Turbulence Research, CNR-ISAC, Sezione di Roma, Via Fosso del Cavaliere 100, 00133 Roma, Italy and INFN, Sezione di Lecce, 73100 Lecce, Italy*
[5]*International Collaboration for Turbulence Research and Max Planck Institute for Dynamics and Self-Organization, Am Fassberg 17, D-37077 Goettingen, Germany*
[6]*International Collaboration for Turbulence Research and Istituto per le Applicazioni del Calcolo CNR, Viale del Policlinico 137, 00161 Roma, Italy and INFN, Sezione di Ferrara, Via G. Saragat 1, I-44100 Ferrara, Italy*

A detailed comparison between data from experimental measurements and numerical simulations of Lagrangian velocity structure functions in turbulence is presented. Experimental data, at Reynolds number ranging from $R_\lambda = 350$ to $R_\lambda = 815$, are obtained in a swirling water flow between counter-rotating baffled disks. Direct numerical simulations (DNS) data, up to $R_\lambda = 284$, are obtained from a statistically homogeneous and isotropic turbulent flow. By integrating information from experiments and numerics, a quantitative understanding of the velocity scaling properties over a wide range of time scales and Reynolds numbers is achieved. To this purpose, we discuss in detail the importance of statistical errors, anisotropy effects, and finite volume and filter effects, finite trajectory lengths. The local scaling properties of the Lagrangian velocity increments in the two data sets are in good quantitative agreement for all time lags, showing a degree of intermittency that changes if measured close to the Kolmogorov time scales or at larger time lags. This systematic study resolves apparent disagreement between observed experimental and numerical scaling properties. © *2008 American Institute of Physics*. [DOI: 10.1063/1.2930672]

I. INTRODUCTION

Understanding the statistical properties of a fully developed turbulent velocity field from the Lagrangian point of view is a challenging theoretical and experimental problem. It is a key ingredient for the development of stochastic models for turbulent transport in such diverse contexts as combustion, pollutant dispersion, cloud formation, and industrial mixing.[1–4] Progress has been hindered primarily by the presence of a wide range of dynamical time scales, an inherent property of fully developed turbulence. Indeed, for a complete description of particle statistics, it is necessary to follow their paths with very fine spatial and temporal resolution, on the order of the Kolmogorov length and time scales η and τ_η. Moreover, the trajectories should be tracked for long times, on the order of the eddy turnover time T_L, requiring access to a vast experimental measurement region. The ratio of the above time scales can be estimated as $T_L/\tau_\eta \sim R_\lambda$, and the Taylor microscale Reynolds number R_λ

ranges from hundreds to thousands in typical laboratory experiments. Despite these difficulties, many experimental and numerical studies of Lagrangian turbulence have been reported over the years.[5–33] Here, we present a detailed comparison between state-of-the-art experimental and numerical studies of high Reynolds number Lagrangian turbulence. We focus on single-particle statistics, with time lags ranging from smaller than τ_η to order T_L. In particular, we study the Lagrangian velocity structure functions (LVSFs), defined as

$$S_p(\tau) = \langle (\delta_\tau v)^p \rangle = \langle [v(t+\tau) - v(t)]^p \rangle, \tag{1}$$

where v denotes a single velocity component.

In the past, the corresponding Eulerian quantities, i.e., the moments of the spatial velocity increments, have attracted significant interest in theory, experiments, and numerical studies (for a review, see Ref. 34). It is now widely accepted that spatial velocity fluctuations are intermittent in the inertial range of scales, for $\eta \ll r \ll L$, L being the largest scale of the flow. By intermittency, we mean anomalous scaling of the moments of the velocity increments, corresponding to a lack of self-similarity of their probability density functions (PDFs) at different scales. In an attempt to explain

a)Authors to whom correspondence should be addressed. Electronic mail: a.lanotte@isac.cnr.it, eberhard.bodenschatz@ds.mpg.de.
b)Present address: Department of Physics, Haverford College, PA 19041.

Eulerian intermittency, many phenomenological theories have been proposed, either based on stochastic cascade models (e.g., multifractal descriptions[35–37]) or on closures of the Navier–Stokes equations.[38] Common to all these models is the presence of nontrivial physics at the dissipative scale, $r \sim \eta$, introduced by the complex matching of the wild fluctuations in the inertial range and the dissipative smoothing mechanism at small scales.[39,40] Numerical and experimental observations show that clean scaling behavior for the Eulerian structure functions is found only in a range $10\eta \leq r \ll L$ (see Ref. 41 for a collection of experimental and numerical results). For spatial scales $r < 10\eta$, multiscaling properties, typical of the intermediate dissipative range, are observed due to the superposition of inertial and dissipative range physics.[40]

Similar questions can be raised in the Lagrangian framework: (i) Is there intermittency in Lagrangian statistics? (ii) Is there a range of time lags where clean scaling properties (i.e., power law behavior) can be detected? (iii) Are there signatures of the complex interplay between inertial and dissipative effects for small time lags $\tau \sim \mathcal{O}(\tau_\eta)$?

In this paper, we shall address the above questions by comparing direct numerical simulations (DNSs) and laboratory experiments. Unlike Eulerian turbulence, the study of which has attracted experimental, numerical, and theoretical efforts since the past 30 years, Lagrangian studies become available only very recently mainly due to the severe difficulty of obtaining accurate experimental and numerical data at sufficiently high Reynolds numbers. Consequently, the understanding of Lagrangian statistics is still poor. This explains the absence of consensus on the scaling properties of the LVSF. In particular, there have been different assessments of the scaling behavior,

$$S_p(\tau) = \langle (\delta_\tau v)^p \rangle \sim \tau^{\xi(p)}, \tag{2}$$

when a *single* number, i.e., the scaling exponent $\xi(p)$, is extracted over a range of time lags.

Measurements using acoustic techniques[10,15] gave the first values of the exponents $\xi(p)$, measuring scaling properties in the range $10\tau_\eta < \tau < T_L$. Subsequently, experiments based on complementary metal oxide semiconductor (CMOS) sensors[26,28] provided access to scaling properties for shorter time lags, $2\tau_\eta \leq \tau \leq 6\tau_\eta$, finding more intermittent values, although compatible with Ref. 10. DNS data, obtained at lower Reynolds number, allowed simultaneous measurements in both of these ranges.[23,29] For $10\tau_\eta \leq \tau \leq 50\tau_\eta$, scaling exponents were found to be slightly less intermittent than those measured with the acoustic techniques, although again compatible within error bars. On the other hand, DNS data[29,33,42] for small time lags, $2\tau_\eta \leq \tau \leq 6\tau_\eta$, agree with scaling exponents measured in Ref. 26.

The primary goal of this paper is to critically compare state-of-the-art numerical and experimental data in order to analyze intermittency at both short, $\tau \approx \tau_\eta$, and intermediate, $\tau_\eta < \tau \ll T_L$, time lags. This is a necessary step both to bring Lagrangian turbulence up to the same scientific standards as Eulerian turbulence and to resolve the conflict between experiment and simulations (see also Refs. 33, 42, and 43).

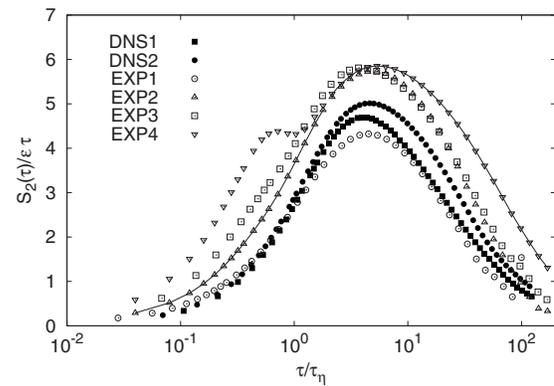To illustrate some of the difficulties discussed above, in

FIG. 1. Log-log plot of the second-order LVSF (averaged over the three components) normalized with the dimensional prediction, i.e., $S_2(\tau)/(\epsilon\tau)$, at various Reynolds numbers and for all data sets. Details can be found in Tables I and II. EXP2 and EXP4 refer to experiments at the same Reynolds number $(R_\lambda = 690)$, but with different measurement volumes (larger in EXP4); in particular, EXP2 and EXP4 better resolve the small and large time lag ranges, respectively, and intersect for $\tau/\tau_\eta \approx 2$. We indicate with a solid line the resulting data set made of data from EXP2 (for $\tau/\tau_\eta < 2$) and EXP4 (for $\tau/\tau_\eta > 2$); a good overlap among these data is observed in the range $2 < \tau/\tau_\eta < 8$. For all data sets, an extended plateau is absent, indicating that the power law regime typical of the inertial range has not yet been achieved, even at the highest Reynolds number, $R_\lambda \sim 815$, in experiment.

Fig. 1, we show a compilation of experimental and numerical results for the second-order Lagrangian structure function at various Reynolds numbers (see later for details). Here and in the following, we consider the LVSF averaged over the three components, so that expression (1) for moment of order p is generalized to $S_p(\tau) = (\frac{1}{3})\Sigma_i \langle (\delta_\tau v_i)^p \rangle$, and the index i runs over the spatial components. The curves are compensated with the dimensional prediction given by the classical Kolmogorov theory in the inertial range,[44] $S_2(\tau) = C_0\epsilon\tau$, where ϵ is the turbulent kinetic energy dissipation. The absence of any extended plateau and the trend with the Reynolds number indicate that the inertial range, if any, has not developed yet. The same trends have been observed in other DNS studies[27] and by analyzing the temporal behavior of signals with a given power law Fourier spectrum.[45]

We stress that assessing the actual scaling behavior of the second (and higher) order LVSFs is crucial for the development of stochastic models for Lagrangian particle evolution. Indeed, these models are based on the requirement that the second-order LVSF scales as $S_2(\tau) \propto \epsilon\tau$. The issues of whether the predicted scaling is ever reached and ultimately how the LVSF deviate as a function of the Reynolds numbers remain to be clarified.

Moreover, an assessment of the presence of Lagrangian intermittency calls for more general questions about phenomenological modeling. For instance, multifractal models derived from Eulerian statistics can be easily translated to the Lagrangian framework[10,23,46,47] with some degree of success.[10,13,18]

The material is organized as follows. In Sec. II, we describe the properties of the experimental setup and the DNSs, detailing the limitations in both sets of data. A comparison of LVSFs is considered in Sec. III. Section III A presents a detailed scale-by-scale discussion of the local scaling exponents, which is the central result of the paper. Section IV

draws conclusions and offers perspectives for the future study of Lagrangian turbulence.

II. EXPERIMENTS AND NUMERICAL SIMULATIONS

Before describing the experimental setup and the DNS, we shall briefly list the possible sources of uncertainties in both experimental and DNS data. In general, this is not an easy task. First, it is important to discern the deterministic from the statistical sources of errors. Second, we must be able to assess the quantitative importance of both types of uncertainties on different observables.

Deterministic uncertainties. For simplicity, we report in this work the data averaged over all three components of the velocity for both the experiments and the DNS. Since neither flows in the experiments nor the DNS are perfectly isotropic, a part of the uncertainty in the reported data comes from the anisotropy. In the experiments, the anisotropy reflects the generation of the flow and the geometry of the experimental apparatus. The anisotropy in DNS is introduced by the finite volume and by the choice of the forcing mechanism. In general, the DNS data are quite close to statistical isotropy, and anisotropy effects are appreciable primarily at large scales. This is also true for the data from the experiment, especially at the higher Reynolds numbers. An important limitation of the experimental data is that the particle trajectories have finite length due both to finite measurement volumes and to the tracking algorithm, which primarily affect the data for large time lags. It needs to be stressed, however, that in the present experimental setup due to the fact that the flow is not driven by bulk forces, but by inertial and viscous forces at the blades, the observation volume would anyhow be limited by the mean velocity and the time it takes for a fluid particle to return to the driving blades. At the blades, the turbulence is strongly influenced by the driving mechanism. Therefore, in the experiments reported here, the observation volume was selected to be sufficiently far away from the blades to minimize anisotropy. For short-time lags, the greatest experimental difficulties come from the finite spatial resolution of the camera and the optics, the image acquisition rate, data filtering, and postprocessing, a step necessary to reduce noise. For DNS, typical sources of uncertainty at small time lags are due to the interpolation of the Eulerian velocity field to obtain the particle position, the integration scheme used to calculate trajectories from the Eulerian data, and the numerical precision of floating point arithmetic.

The *statistical uncertainties* for both the experimental and DNS data arise primarily from the finite number of particle trajectories and—especially for DNS—from the time duration of the observation. We note that this problem is also reflected in a residual, large-scale anisotropy induced by the nonperfect averaging of the forcing fluctuations in the few eddy turnover times simulated. The number of independent flow realizations can also contribute to the statistical convergence of the data. While it is common to obtain experimental measurements separated by many eddy turnover times, typical DNS results contain data from at most a few eddy turnover times.

We stress that, particularly for Lagrangian turbulence,

only an in-depth comparison of experimental and numerical data will allow the quantitative assessment of uncertainties. For instance, as we shall see below, DNS data can be used to investigate some of the geometrical and statistical effects induced by the experimental apparatus and measurement technique. This enables us to quantify the importance of some of the above mentioned sources of uncertainty directly. DNS data are, however, limited to smaller Reynolds number than experiment; therefore, only data from experiments can help to better quantify Reynolds number effects.

A. Experiments

The most comprehensive experimental data of Lagrangian statistics are obtained by optically tracking passive tracer particles seeded in the fluid. Images of the tracer particles are analyzed to determine their motion in the turbulent flow.[6,7,48] Due to the rapid decrease of the Kolmogorov scale with Reynolds number in typical laboratory flows, previous experimental measurements were often limited to small Reynolds numbers.[6,8] The Kolmogorov time scale at $R_\lambda \sim 10^3$ in a laboratory water flow was so far resolved only by using four high speed silicon strip detectors originally developed for high-energy physics experiments.[9,11] The one-dimensional nature of the silicon strip detector, however, restricted the three-dimensional tracking to a single particle at a time, limiting severely the rate of data collection. Recent advances in electronics technology now allow simultaneous three-dimensional measurements of $\mathcal{O}(10^2)$ particles at a time by using three cameras with two-dimensional CMOS sensors. High-resolution Lagrangian velocity statistics at Reynolds numbers comparable to those measured using silicon strip detectors are therefore becoming available.[26]

Lagrangian statistics can also be measured acoustically. The acoustic technique measures the Doppler frequency shift of ultrasound reflected from particles in the flow, which is directly proportional to their velocity.[10,15] The size of the particles needed for signal strength in the acoustic measurements can be significantly larger than the Kolmogorov scale of the flow. Consequently, the particles do not follow the motion of fluid particles,[11] and this makes the interpretation of the experimental data more difficult.[15]

The experimental data here presented are discussed in much detail in Refs. 26 and 28. In the following, we only briefly recall the main aspects of the experimental technique and data sets, whose parameters are summarized in Table I. Turbulence was generated in a swirling water flow between counter-rotating baffled disks in a cylindrical container. The flow was seeded with polystyrene particles of size $d_p = 25$ μm and density $\rho_p = 1.06$ g/cm^3 that follow the flow faithfully for R_λ up to 10^3.[11] The particles were illuminated by high-power Nd:YAG lasers, and three cameras at different viewing angles were used to record the motion of the tracer particles in the center of the apparatus. Images were processed to find particle positions in three-dimensional physical space; the particles were then first tracked using a predictive algorithm to obtain the Lagrangian trajectories.[48] Due to fluctuations in laser intensity, the uneven sensitivity of the physical pixels in the camera sensor array, plus electronic

TABLE I. Parameters of the experiments. Column 2 gives the Taylor microscale Reynolds numbers taken from previous experiments (Ref. 11) in the same flow generating apparatus at the same driving speeds of the motors reported here. In Ref. 11, a small volume $\sim (2 \text{ mm})^3$ at the center of the apparatus was measured, while the measurement volumes in the current experiments were $\sim (2 \text{ cm})^3$ and $\sim (5 \text{ cm})^3$. We found that the local velocity fluctuations, measured in subvolumes with size of $(2 \text{ mm})^3$, varied by 5%–10%. This might be attributed to statistical convergence (typically $\sim 10^5$ samples in each subvolume) and possibly to the inhomogeneity of the flow. At the center of the apparatus, the fluctuation velocity was the highest and agreed with the value reported in Ref. 11. The fluctuation velocities reported in column 3 are the spatial averages over the entire measurement volume. They are approximately 5% lower than the values given in Ref. 11. Since $R_\lambda \propto v_{\text{rms}}'^2$, a 5% difference in v_{rms}' corresponds to a 10% difference in R_λ. Column 3 gives the value of the root-mean-square velocity fluctuations v_{rms}' averaged over the three components. The integral length scale $L \equiv v_{\text{rms}}'^3 / \varepsilon = 7$ cm was determined to be independent of Reynolds number. $T_L \equiv L / v_{\text{rms}}'$ is the eddy turnover time. N_f is the temporal resolution of the measurement in units of frames per τ_η. The measurement volume was nearly a cube in the center of the tank and its linear dimensions are given in units of the integral length scale L. Δx is the spatial discretization of the recording system. The spatial uncertainty of the position measurements is roughly $0.1 \Delta x$. N_R is the number of independent realizations recorded (see text). N_{tr} is the number of Lagrangian trajectories measured. We note that the energy dissipation rate was inferred from measurements of the second-order Eulerian structure functions.

No.	R_λ	v'_{rms} (m/s)	ε (m²/s³)	η (μm)	τ_η (ms)	T_L (s)	N_f (f/τ_η)	Measured volume in (L^3)	Δx (μm/pix)	N_R	N_{tr}
EXP1	350	0.11	2.0×10^{-2}	84	7.0	0.63	35	$0.4 \times 0.4 \times 0.4$	50	500	9.3×10^5
EXP2	690	0.42	1.2	30	0.90	0.16	24	$0.3 \times 0.3 \times 0.3$	80	480	9.6×10^5
EXP3	815	0.59	3.0	23	0.54	0.11	15	$0.3 \times 0.3 \times 0.3$	80	500	1.7×10^6
EXP4	690	0.42	1.2	30	0.90	0.16	24	$0.7 \times 0.7 \times 0.7$	200	1200	6.0×10^6

and thermal noise, images of particles sometimes fluctuate and appear to blink. When the image intensity of a particle was too low, the tracking algorithm lost that particle. Consequently, the trajectory of that particle was terminated. When the image intensity is high again, the algorithm started a new trajectory. The raw trajectories therefore contained many short segments that in reality belonged to the same trajectory. It is, however, possible to connect these segments by applying a predictive algorithm in the six-dimensional space of coordinates and velocities. The trajectories discussed in this paper were obtained with the latter method, which allows for much longer tracks.

The Lagrangian velocities were calculated by smoothing the measured positions and subsequently differentiating. A Gaussian filter has been used to smooth the data. Smoothing and differentiation can be combined into one convolution operation by integration by parts; the convolution kernel is simply the derivative of the Gaussian smoothing filter.[16] The width of the Gaussian kernel was chosen to remove the noise in position measurements, but not to suppress the fluctuations, whose characteristic time scale is $\mathcal{O}(\tau_\eta)$ or above. The velocity statistics have been found to be insensitive to the width σ of the Gaussian filter, provided that it is between $\tau_\eta/6$ and $\tau_\eta/3$ (see also below). The temporal resolution of the camera system in the experiments reported here was sufficiently high to ensure that the fluctuations with time scale greater than $\tau_\eta/6$ were well resolved.

The uncertainty in position measurement, or the spatial resolution, is directly proportional to the size of the spatial discretization determined by the optical magnification and by the size of the pixels on the CMOS sensor. Larger magnification gives better spatial resolution but also a smaller measurement volume. Indeed, the number of usable pixels of the camera sensor array is fixed by the chip size and, at higher speeds, by the imaging rate. The dynamic range of the cameras is not sufficient to cover the entire range of scales of the turbulence at the Reynolds numbers of interest. Therefore, two sets of experiments with different magnifications have been performed. The former set has a high spatial resolution

and focuses on the small scale quantities, although with a relatively small measurement volume (EXP1, 2, and 3 in Table I). Then, in order to probe longer times and larger scales, the size of the measurement volume in the second set of measurements was chosen to be slightly smaller than the integral scale (EXP4 in Table I). In this data set, however, the uncertainty in position was larger and the short-time statistics were severely affected. As a result, in order to have experimental data covering a wide range of time lags ($\tau_\eta \lesssim \tau \lesssim 100\tau_\eta$) at a given Reynolds number, one needs to merge data from the two different experiments. This could be done at $R_\lambda = 690$ by using data from the small measurement volume (EXP2) up to times $\tau \sim (6-7)\tau_\eta$ and using data from large measurement volume (EXP4) at larger times. The procedure is well justified as the two data sets match for intermediate time lags.

One noticeable difference between experiments and numerical simulations is the number of independent realizations included in the statistics. While it is difficult to have many statistically independent DNS results at one Reynolds number, the experimental data usually contained $\mathcal{O}(10^3)$ records separated by a time interval of about $10^2 T_L$. Each of these records lasted for $(1-2)T_L$. The variation of the velocity fluctuations calculated from the statistics of many records is shown in Fig. 2(a). As it is clear from it, the three components do not fluctuate about the same value, indicating the presence of anisotropy, which does not average away even after many eddy turnover times. These effects are introduced by the flow generation in the apparatus. In the following, the uncertainties in the data sets due to anisotropy were estimated by the difference between measurements made on different components of the velocity field.

B. DNS

Nowadays, state-of-the-art numerics[19,23,49,50] best suited for Eulerian statistics is able to reach Taylor scale Reynolds numbers of the order of $R_\lambda \sim 1000$ by using up to 4096^3 mesh points.[50] Such extremely high Reynolds number DNS
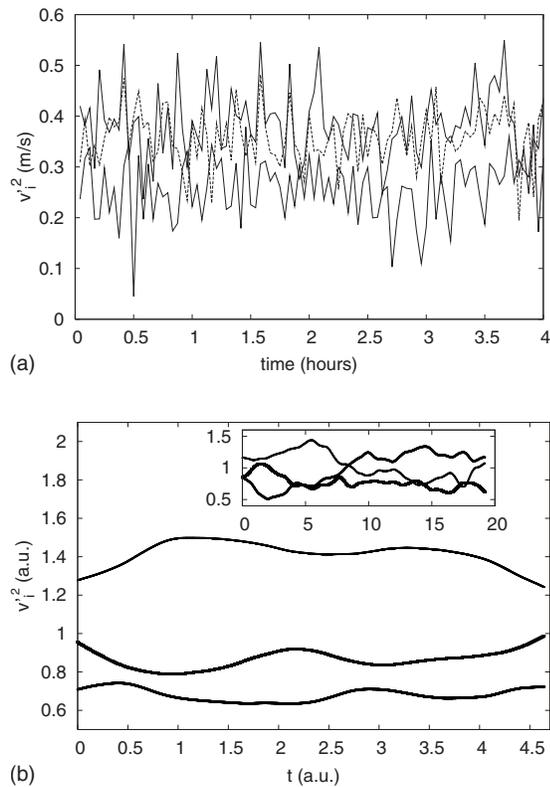
FIG. 2. (a) Time evolution of the components of the velocity fluctuation $v_x'^2$ (dashed line), $v_y'^2$ (thick black line), and $v_z'^2$ (solid line) for EXP2. (b) Time evolution of velocity fluctuations $v_i'^2$, with $i=x,y,z$, for DNS2. In the inset, we show the same time evolution for a DNS at a smaller $R_\lambda \approx 75$ (obtained with a spatial resolution of 128^3 grid points and the same forcing), which was integrated for a much longer time. In the latter case, the three components fluctuate around the same value, showing the recovery of isotropy for long enough time.

is, however, limited by the impossibility of integrating the flow for long time durations, due to the extremely high computational cost. In Lagrangian studies, it is necessary to highly resolve the Eulerian velocity field to obtain precise out-of-grid interpolation. The maximum achievable Reynolds number, on the fastest computers, is currently limited to $R_\lambda \sim 600$ in order to accurately calculate the particle positions and to achieve sufficiently long integration times.[4,19,23,27]

Typically, such Lagrangian simulations last for a few large-scale eddy turnover times, implying some unavoidable remaining anisotropy at large scales, even for nominally perfectly isotropic forcing. The simulations analyzed here were forced by fixing the total energy of the first two Fourier-space shells:[51] $E(k_1)=\Sigma_{|\boldsymbol{k}| \in I_1}|\hat{v}(\boldsymbol{k})|$ and $E(k_2)=\Sigma_{|\boldsymbol{k}| \in I_2}|\hat{v}(\boldsymbol{k})|$, where $I_1=[0.5:1.5]$ and $I_2=[1.5:2.5]$ (the $|\boldsymbol{k}|=0$ mode is fixed to zero to avoid a mean flow). The three velocity components can instantaneously be quite different: when one of the three fluctuates, the others must compensate in order to keep the total amplitude fixed [see, for instance, Fig. 2(b) for a visualization of this effect]. However, by averaging over many eddy turnover times—when possible, as for the lower-resolution DNS shown in the inset of Fig. 2(b)—the forcing produces a perfectly statistically isotropic flow. As the remaining large-scale anisotropy is the main source of uncer-

tainty in the DNS results, we will estimate confidence intervals from the difference between the three components.

In the simulations, the main systematic error for small time lags comes from the interpolation of the Eulerian velocity fields needed to integrate the equation for particle positions,

$$\dot{X}(t) = \boldsymbol{v}[X(t),t]. \tag{3}$$

Of course, high-order interpolation schemes such as third-order Taylor series interpolation or cubic splines, now currently used in parallel codes, partially remove this problem.[27] If we compare DNS with the same value of $k_{\max}\eta$, where $k_{\max}$ is the maximum wavenumber resolved, cubic splines give higher interpolation accuracy. It has been reported[52] that cubic schemes may resolve the most intense events better than linear interpolation, especially for acceleration statistics; the effect, however, appears to be rather small especially as far as velocity is concerned.

More crucial than the order of the interpolation scheme is the resolution of the Eulerian grid in terms of the Kolmogorov length scale. To enlarge the inertial range as much as possible, pure Eulerian simulations may not resolve the smallest scale velocity fluctuations sufficiently well, by choosing a grid spacing Δx larger than the Kolmogorov scale η. Since this strategy may be particularly harmful to Lagrangian analysis, here it has been chosen to better resolve the smallest fluctuations by choosing $\Delta x \simeq \eta$ and to use the simple and computationally less expensive linear interpolation.

We stress that having well resolved dissipative physics for the Eulerian field is also very important for capturing the formation of rare structures on a scale $r \approx \eta$. Moreover, as discussed in Ref. 53, such structures, because of their filamentary geometry, may influence not only viscous but also inertial range physics.

Another possible source of error comes from the loss of accuracy in the integration of Eq. (3) for very small velocities due to round-off errors. This problem can be overcome by adopting higher-order schemes for temporal discretization. For extremely high Reynolds numbers, it may also be necessary to use double precision arithmetic, while for moderate R_λ, single precision, which was adopted in the present DNS, is sufficient for accurate results (see, e.g., Ref. 52). We also remark that in our runs, round-off errors are always subleading with respect to errors coming from interpolation or temporal discretization schemes.

Details of the DNS analyzed here can be found elsewhere;[23] here, we simply state that the Lagrangian tracers move according to Eq. (3), in a cubic, triply periodic domain of side $\mathcal{B}=2\pi$. DNS parameters are summarized in Table II.

III. COMPARISON OF LAGRANGIAN STRUCTURE FUNCTIONS

Let us now compare the experimental and numerical measurements of the LVSFs directly. Figures 3(a) and 3(b) show a direct comparison of LVSFs of order $p=2$ and $p=4$

TABLE II. Parameters of the numerical simulations. Taylor microscale Reynolds number $R_\lambda \equiv \sqrt{15} v_{rms}'^2 / \sqrt{\epsilon \nu}$, root-mean-square velocity fluctuations v_{rms}' $= 2E/3$, where E is the kinetic energy, energy dissipation ϵ, viscosity ν, Kolmogorov length scale $\eta = (\nu^3/\epsilon)^{1/4}$, integral scale L equal to half side of the numerical box, large-eddy turnover time $T_L = L/v_{rms}'$, Kolmogorov time scale $\tau_\eta = (\nu/\epsilon)^{1/2}$, total integration time T, grid spacing Δx, resolution N^3, and the number of Lagrangian tracers N_p. In the DNS, energy dissipation is measured as $\epsilon = 15\nu \langle (\partial_z v_z)^2 \rangle$. Note that the values of v_{rms}' and of T differ from those reported in Ref. 23, where these values were misprinted.

No.	R_λ	v_{rms}'	ϵ	ν	η	L	T_L	τ_η	T	Δx	N^3	N_p
DNS1	178	1.4	0.886	0.002 05	0.01	3.14	2.2	0.048	5	0.012	512^3	0.96×10^6
DNS2	284	1.4	0.81	0.000 88	0.0054	3.14	2.2	0.033	4.4	0.006	1024^3	1.92×10^6

for all data sets. The curves are plotted using the standard Kolmogorov scaling, which assumes that in the inertial range,

$$S_2(\tau) \propto \epsilon \tau \propto v_{rms}'^2 R_\lambda^{-1}(\tau/\tau_\eta)$$

[where we have used the following relations: $\epsilon \propto v_{rms}'^3 / L$ (Ref. 54) and $T_L / \tau_\eta \propto R_\lambda$]. Such a formulation can be generalized to $S_p(\tau) \propto v_{rms}'^p R_\lambda^{-p/2}(\tau/\tau_\eta)^{p/2}$. Both the second- and fourth-order moments show a fairly good collapse, especially in the range of intermediate time lags. However, some dependence can be observed both on R_λ [see Fig. 3(b)] and on the size of the measurement volume (compare EXP2 and EXP4). Both effects call for a more quantitative understanding.
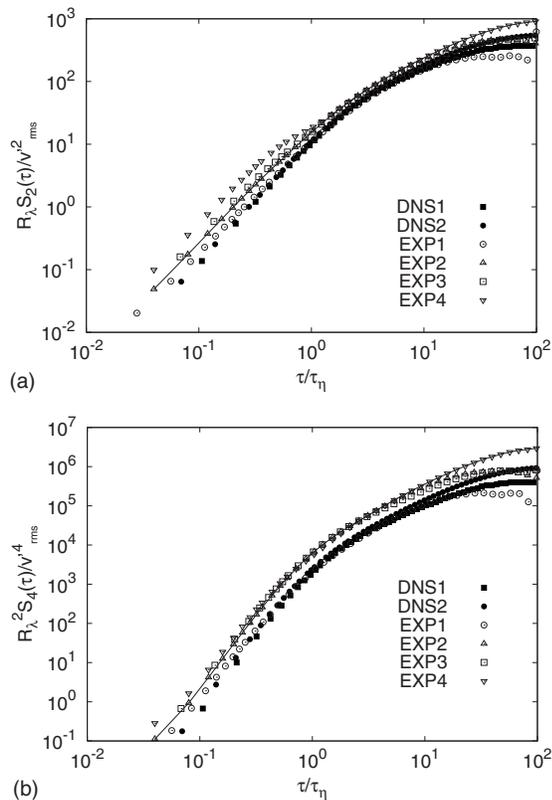

FIG. 3. (a) Log-log plot of the second-order structure function compensated as $R_\lambda S_2(\tau)/v_{rms}'^2$ vs τ/τ_η for all data sets at several Reynolds numbers. (b) The same for the fourth-order structure function $R_\lambda^2 S_4(\tau)/v_{rms}'^4$. The solid line is made to guide the eyes through the two data sets (EXP2 and EXP4) obtained at the same Reynolds number in two different measurement volumes, as explained in Sec. II A.

A. Local scaling exponents

A common way to assess how the statistical properties change for varying time lags is to look at dimensionless quantities such as the generalized flatness,

$$F_{2p}(\tau) = \frac{S_{2p}(\tau)}{[S_2(\tau)]^p}. \quad (4)$$

We speak of *intermittency* when such a function changes its behavior as a function of τ. This is equivalent to the PDF of the velocity fluctuations $\delta_\tau v$, normalized to unit variance, changing shape for different τ.[34]

When the generalized flatness varies with τ as a power law, $F_{2p}(\tau) \sim \tau^{\chi(2p)}$, the scaling laws are *intermittent*. Such behavior is very difficult to assess quantitatively since many decades of scaling are typically needed to remove the effects of subleading contributions (for instance, it is known that Eulerian scaling may be strongly affected by slowly decaying anisotropic fluctuations[56]).

We are interested in quantifying the degree of intermittency at changing τ. In Fig. 4, we plot the generalized flatness $F_{2p}(\tau)$ for $p=2$ and $p=3$ for the data sets DNS2, EXP2, and EXP4. Numerical and experimental results are very close and clearly show that the intermittency changes considerably going from small to large τ.
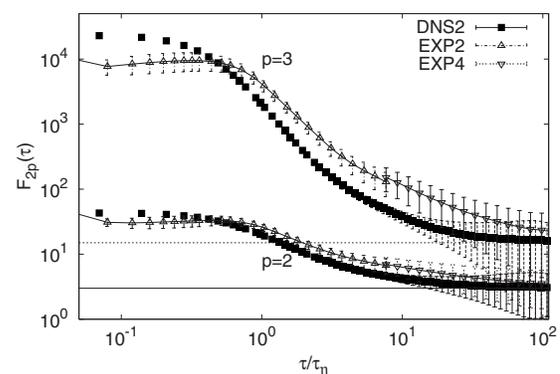

FIG. 4. Generalized flatness $F_{2p}(\tau)$ of order $p=2$ and $p=3$ measured from DNS2, EXP2, and EXP4. Data from EXP2 and EXP4 are connected by a continuous line. The Gaussian values are given by the two horizontal lines. The curves have been averaged over the three velocity components and the error bars (Ref. 55) shown here are computed from the scatter between the three different components as a measure of the effect of anisotropy. Statistical errors due to the limitation in the statistics have been also evaluated by dividing the whole data sets in subsamples and comparing the results. These statistical errors are always smaller than those plotted here, which were estimated from the residual anisotropy.

The difficulty in trying to characterize these changes quantitatively is that, as shown by Fig. 4, one needs to capture variations over many orders of magnitude. For this reason, we prefer to look at observables that remain $\mathcal{O}(1)$ over the entire range of scales and which convey information about intermittency *without having to fit any scaling exponent*. With this aim, we measured the logarithmic derivative (also called local slope or local exponent) of structure function of order p, $S_p(\tau)$, with respect to a reference structure function,[57] for which we chose the second-order $S_2(\tau)$,

$$\zeta_p(\tau) = \frac{d \log[S_p(\tau)]}{d \log[S_2(\tau)]}. \tag{5}$$

We stress the importance of taking the derivative with respect to a given moment: this is a direct way of looking at intermittency with no need of *ad hoc* fitting procedures and no request of power law behavior. This procedure,[57] which goes under the name of extended self-similarity[57] (ESS), is particularly important when assessing the statistical properties at Reynolds numbers not too high and/or close to the viscous dissipative range.

A nonintermittent behavior would correspond to $\zeta_p(\tau) = p/2$. In the range of τ for which the exponents $\zeta_p(\tau)$ are different from the dimensional values $p/2$, structure functions are intermittent and correspondingly the normalized PDFs of $(\delta_\tau v / \langle (\delta_\tau v)^2 \rangle^{1/2})$ change shape with τ. Figures 5(a) and 5(b) show the logarithmic local slopes of the numerical and experimental data sets for several Reynolds numbers for $p=4$ and $p=6$ versus time normalized to the Kolmogorov scale, τ/τ_η. These are the main results of our analysis.

The first observation is that for both orders $p=4$ and $p=6$, the local slopes $\zeta_p(\tau)$ deviate strongly from their nonintermittent values $\zeta_4=2$ and $\zeta_6=3$. There is a tendency toward the differentiable nonintermittent limit $\zeta_p=p/2$ only for very small time lags $\tau \ll \tau_\eta$. In the following, we shall discuss in detail the small and larger time lag behavior, where by large, we mean $\tau_\eta < \tau \ll T_L$.

Small time lags. For the structure function of order $p=4$ [Fig. 5(a)], we observe the strongest deviation from the nonintermittent value in the range of time $2\tau_\eta \lesssim \tau \lesssim 6\tau_\eta$. It has previously been proposed that this deviation is associated with particle trapping in vortex filaments.[23] This fact has been supported by DNS investigations of inertial particles.[14,17,29] The agreement between the DNS and the experimental data in this range is remarkable. For $p=6$ [Fig. 5(b)], the scatter among the data is higher due to the fact that with increasing order of the moments, inaccuracies in the data become more important. Still, the agreement between DNS and the experimental data is excellent. Differently from the $p=4$ case, a dependence of mean quantities on the Reynolds number is here detectable, although it lies within the error bars. The experimental data set for $p=6$, at the highest Reynolds number ($R_\lambda=815$), shows a detectable trend in the local slope toward less intermittent values in the dip region, $2 \lesssim \tau/\tau_\eta \lesssim 6$. This change may potentially be the signature of vortex destabilization at high Reynolds number—which would reduce the effect of vortex trapping. It is more likely, however, that at this very high Reynolds number, both spatial
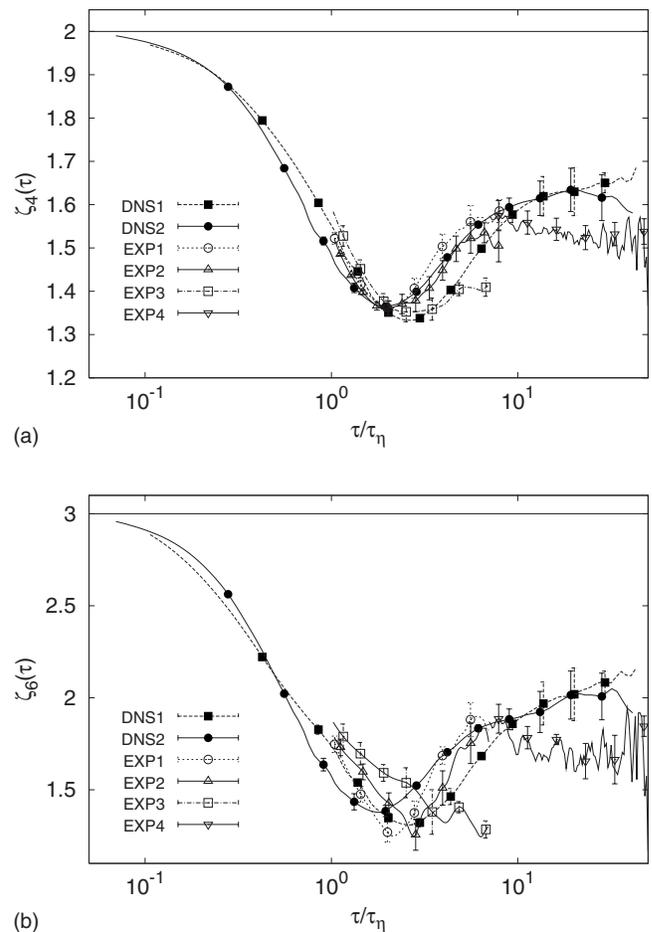

(a)

(b)

FIG. 5. Logarithmic derivatives $\zeta_p(\tau)$ of structure functions $S_p(\tau)$ with respect to $S_2(\tau)$ for orders $p=4$ (a) and $p=6$ (b). The curves are averaged over the three velocity components and the error bars are computed from the statistical (anisotropic) fluctuations between LVSFs of different components. The horizontal lines are the nonintermittent values for the logarithmic local slopes, i.e., $\zeta_p=p/2$. We stress that the curves for EXP1, 2, and 3 are shown in the time range $1 \le \tau/\tau_\eta \le 7$, while the curves for EXP4 (large measurement volume) are shown in the time range $7 \le \tau/\tau_\eta \le 50$.

and temporal resolution of the measurement system may not have been sufficient to resolve the actual trajectories of intense events.[23] We consider this to be an important open question for future studies.

Larger time lags. For τ larger than $(6-7)\tau_\eta$ up to T_L, the experimental data obtained in small measurement volumes (EXP1, 2, and 3) are not resolving the physics, as they develop both strong oscillations and a common trend toward smaller and smaller values for the local slopes for increasing τ. This may be attributed to the finite measurement volume effect (see also Sec. III B). For these reasons, the data of EXP1, 2, and 3 are not shown for these time ranges. On the other hand, the data from EXP4, obtained from a larger measurement volume, allow us to compare experiment and simulation. Here, the local slope of the experimental data changes slower very much akin to the simulations. This suggests that in this region, high Reynolds number turbulence may show a plateau, although the current data cannot give a definitive answer to this question. For $p=6$, a similar trend is detected, although with larger uncertainties. The excellent quantitative agreement between DNS and the experimental data gives us

high confidence into the local slope behavior as a function of time lag.

In light of these results, we can finally clarify the recent apparent discrepancy between measured scaling exponents of the LVSFs in experiments[26] and DNS,[23] which have lead to some controversy in the literature.[33,42,43] In the experimental work,[26] scaling exponents were measured by fitting the curves in Fig. 5 in the range $2\tau_\eta \lesssim \tau \lesssim 6\tau_\eta$, where the compensated second-order velocity structure functions reach a maximum, as shown in Fig. 1 [measuring the fourth- and sixth-order scaling exponents $\zeta_p(\tau)$ to be 1.4 ± 0.1 and 1.6 ± 0.1, respectively]. On the other hand, in the simulations,[23] scaling exponents were measured in the regions in the range of times $10\tau_\eta \lesssim \tau \lesssim 50\tau_\eta$ (finding the values $\zeta_4 = 1.6 \pm 0.1$ and $\zeta_6 = 2.0 \pm 0.1$).

It needs to be emphasized, however, that the limits induced by the finiteness of volume and of the inertial range extension in both DNS and experimental data do not allow for making a definitive statement about the behavior in the region $\tau > 10\tau_\eta$. We may ask instead if the relative extension of the interval where we see the large dip at $\tau \sim 2\tau_\eta$ and the possible plateau, observed for $\tau > 10\tau_\eta$ both in the numerical and experimental data (see EXP4 data set), become larger or smaller at increasing the Reynolds number.[32] If the dip region—the one presumably affected by vortex filaments—flattens, it would give the asymptotically stable scaling properties of Lagrangian turbulence. If instead the apparent plateau region, at large times, increases in size while the effect of high intensity vortex remains limited to time lags around $(2-6)\tau_\eta$, the plateau region would give the asymptotic scaling properties of Lagrangian turbulence. This point remains a very important question for the future because, as of today, it cannot be answered conclusively either by experiments or by simulations.

B. Finite volume effects at large time lags

As noted above, the EXP4 data for $\zeta_4(\tau)$ develop an apparent plateau at a smaller value than the DNS data. In this section, we show how the DNS data can be used to suggest a possible origin for this mismatch.

We investigate the behavior of the local slopes for the simulations when the volume of size $\mathcal{L}^3$, where particles are tracked, is systematically decreased. We consider in the analysis only trajectories which stay in subvolume of size $\mathcal{L}^3$, so partly mimicking what happens in the experimental measurement volume. We consider volume sizes in the range that goes from the full box size with side $\mathcal{B}$ to boxes with side $\mathcal{L} = \mathcal{B}/7$, and we average over all the sub-boxes to increase the statistical samples. In Fig. 6, we plot the statistics of the trajectory durations for both the experiment and DNS2 by varying the measurement volume size.

As shown in Ref. 58, the probability of the trajectory durations in finite volume measurements is independent of the size of the measurement volume if the trajectory duration is normalized by the residence time $T_{res} = \mathcal{L}/v'_{rms}$, which is the case in Fig. 6(a) for DNS data. For the experimental trajectories, if the residence time is estimated from the geometrical side B_{obs} of the measurement volume as T_{res}
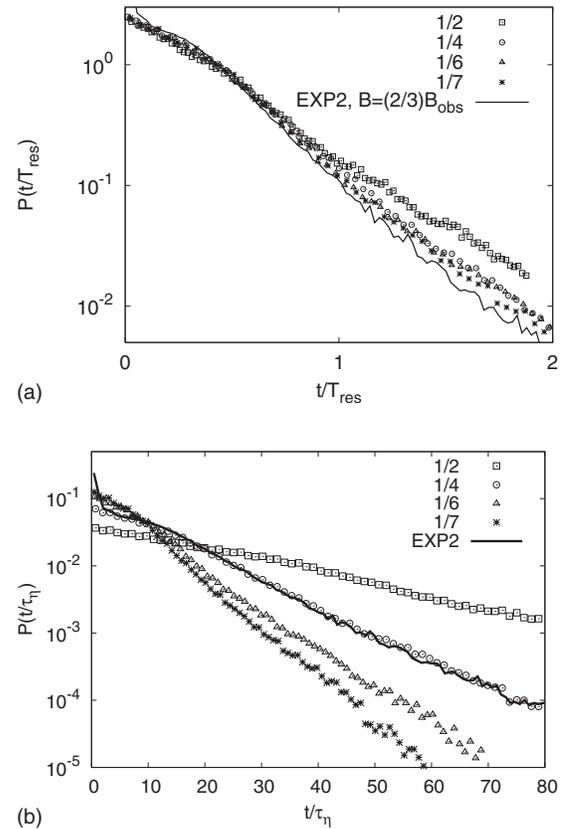

FIG. 6. (a) Comparison of the probability $\mathcal{P}(t/T_{res})$ that a trajectory lasts a time t vs t/T_{res} for the experiment EXP2 and for DNS2 trajectories measured in different numerical measurement domains $\mathcal{L}/\mathcal{B} = \frac{1}{2}, \frac{1}{4}, \frac{1}{6}, \frac{1}{7}$, where T_{res} is the residence time and $\mathcal{L} = 2\pi$ is the computational box. For DNS trajectories, T_{res} is determined from the size of the subdomain as $T_{res} = L/v'_{rms}$. For experimental trajectories, $T_{res} = (\frac{2}{3})B_{obs}/v'_{rms}$, where B_{obs} is the size of the measurement volume, as given in Table I. Data for $t/T_{res} > 2$, for DNS at $\mathcal{L}/\mathcal{B} = \frac{1}{4}, \frac{1}{6}, \frac{1}{7}$ and for the experiment, have been cut out. (b) Comparison of the probability $\mathcal{P}(t/\tau_\eta)$ that a trajectory lasts a time t vs t/τ_η for the same data as before.

$= B_{obs}/v'_{rms}$, the curve is off from others. This is explained by fact that experimental trajectories might still terminate prematurely for the reasons discussed in Sec. II A. Even after an attempt was made to connect trajectory segments, the effective residence time could be smaller than that determined from the geometrical size of the measurement volume. In Fig. 6(a), we show indeed that the probability for experimental trajectories collapses with DNS curves, if we reduce the effective side of the measurement box to $(\frac{2}{3})B_{obs}$ or $T_{res} = (\frac{2}{3})B_{obs}/v'_{rms}$. From the same plot, we might also notice that the DNS curve for $\mathcal{L} = \mathcal{B}/2$, which has the largest residential time T_{res}, slightly departs from the others. This is due to statistics since those points that deviate belong to the tails of the distribution, where we do not expect a perfect collapse.

Finally, comparing T_{res}/τ_η then indicates that EXP2 could be compared to DNS2 with subdomain of side $\mathcal{B}/4$, as shown in Fig. 6(b). Here, we are implicitly assuming that even if particle track loss might have a different origin in the experiment (optical and finite volume effects) and in the numerics (only finite volume effect), the resulting statistics is biased in a similar way. Also, we are assuming that Reynolds
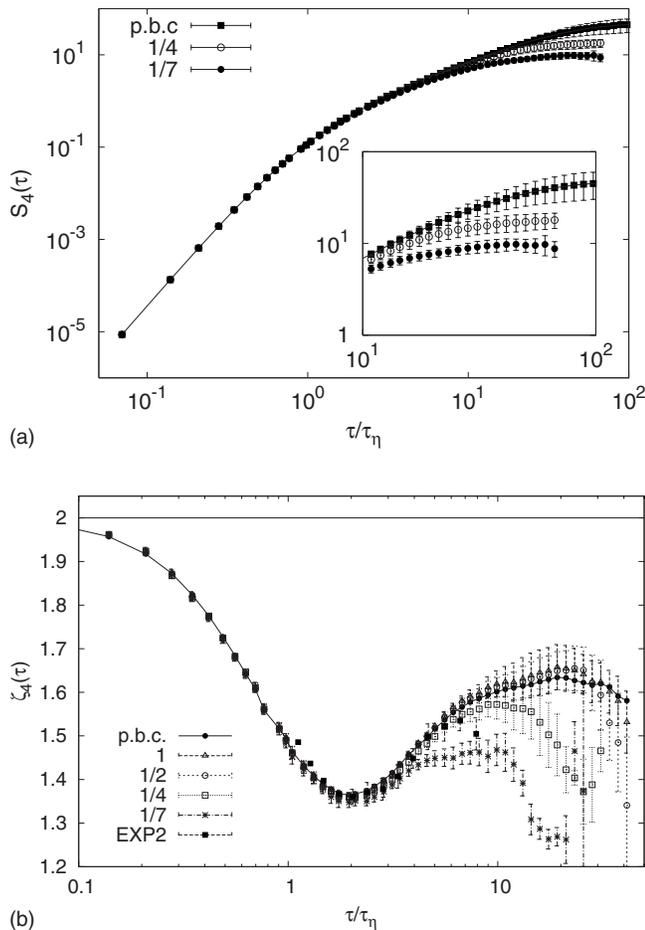
FIG. 7. (a) The fourth-order structure function $S_4(\tau)$ vs τ/τ_η measured from DNS2 trajectories for both full length trajectories (and with periodic boundary conditions) and for trajectories in smaller measurement volumes $L/\mathcal{B} = \frac{1}{4}, \frac{1}{7}$. (b) The logarithmic local slope $\zeta_4(\tau)$ measured from DNS2 trajectories for both the full length trajectories (periodic boundary conditions) and for trajectories in smaller measurement volumes $L/\mathcal{B} = 1, \frac{1}{2}, \frac{1}{4}, \frac{1}{7}$. Note the tendency toward a less developed plateau, at smaller and smaller values, as the measurement volume decreases. In the same plot, we also compare the local slope of EXP2, whose trajectory length distribution is well reproduced by DNS2 data in the subvolume $\mathcal{L}/\mathcal{B} = \frac{1}{4}$.

dependence is well accounted for by normalizing the residence time with the Kolmogorov time scale. A deeper analysis of these issues is left to future work.

It is now interesting to look at the LVSF measured from these finite length numerical trajectories. In Fig. 7(a), we show the fourth-order LVSF obtained by considering the full length trajectories and the trajectories living in a subvolume as explained above. What clearly appears from Fig. 7(a) is that the finite length of the trajectories lowers the value of the structure functions for time lags of the order of $20\tau_\eta \lesssim \tau \lesssim 40\tau_\eta$. Indeed, the finite-length statistics give a signal that is always lower than the full averaged quantity: this effect may be due to a bias to slow, less energetic particles, which have a tendency to linger inside the volume for longer times than fast particles, introducing a systematic change in the statistics. Note that this is the same trend detected when comparing EXP2 and EXP4 in Fig. 3. In Fig. 7(b), we also show the effect of the finite measurement volume on the local slope for $p=4$. By decreasing the observation volume,

we observe a trend in the local slope toward a shorter and shorter plateau with smaller and smaller values. In the same figure, we also compare the logarithmic local slope of EXP2: the residence time analysis shows that EXP2 should be compared to DNS2 data in the subvolume with side $\mathcal{L} = \mathcal{B}/4$. We observe that at scales where both signals are present, the trend is similar. However, we have to remember that in experiment, particles are lost when exiting the measurement volume (finite volume effect) but also inside the measurement volume due to optical particle tracking limitations. This may explain the small discrepancy in Fig. 7(b), among the EXP2 and the $\mathcal{L} = \mathcal{B}/4$ DNS2 signal. More generally, we think that the loss of particles could be the source of the small offset between the plateaus developed by the EXP4 data and the DNS data in Fig. 5.

For the sake of clarity, we should recall that in the DNS, particles can travel across a cubic fully periodic volume, so during their full history they can re-enter the volume several times. In principle, this may affect the results for long time delays. However, since the particle velocity is taken at different times, we may expect possible spurious correlations induced by the periodicity to be very small, if not absent. This is indeed confirmed in Fig. 7(b) where we can notice the perfect agreement between data obtained by using periodic boundary conditions or limiting the analysis to subvolumes of side $\mathcal{L} = \mathcal{B}$ (i.e., not retaining the periodicity) and even $\mathcal{L} = \mathcal{B}/2$.

C. Filtering and measurement error effects at small time lags

As discussed in Sec. II, results at small time lags can be slightly contaminated by several effects both in DNS and experiments. DNS data can be biased by resolution effects due to interpolation of the Eulerian velocity field at the particle position. In experiments, uncorrelated experimental noise needs to be filtered to recover the trajectories.[7,11,16]

To understand the importance of such effects quantitatively, we have modified the numerical Lagrangian trajectories in the following way. First, we have introduced a random noise of the order of $\eta/10$ to the particle position in order to mimic the noise present in the experimental particle detection. Second, we have implemented the same Gaussian filter of variable width used to smooth the experimental trajectories $x(t)$. We also tested the effect of filtering by processing experimental data with filters of different lengths.

In Figs. 8(a) and 8(b), we show the local scaling exponents for $\zeta_4(\tau)$, as measured from these modified DNS trajectories together with the results obtained from the experiment, for several filter widths. The qualitative trend is very similar for both the DNS and the experiment. The noise in particle position introduces nonmonotonic behavior in the local slopes at very small time lags in the DNS trajectories. This effect clearly indicates that small scale noise may strongly perturb measurements at small time lags but will not have important consequences for the behavior on time scales larger than τ_η. On the other hand, the effect of the filter is to slightly increase the smoothness at small time lags (notice that the shift of local slopes curves toward the right for τ
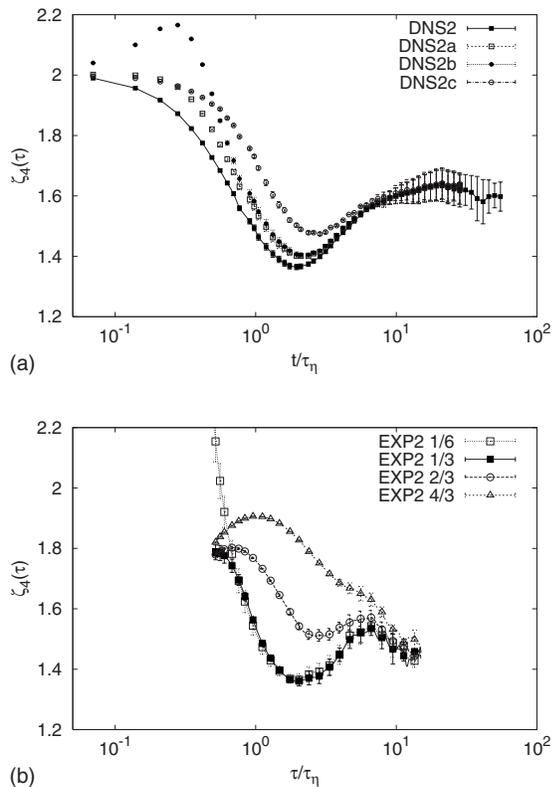
FIG. 8. (a) Logarithmic local slope $\zeta_4(\tau)$ for the DNS2 data set. The symbols DNS2a, b, and c denote the DNS2 trajectories modified by noise and filter effects, mimicking the processing of experimental data. In particular, DNS2a refers to the introduction of noise in the particle position of the order of $\delta x \sim \eta/10$ and with a Gaussian filter width $\sigma \sim \tau_\eta/3$, DNS2b to the same filter width but with much larger spatial noise ($\delta x \sim \eta/4$), and DNS2c to the same spatial noise but a large filter width $\sigma \sim 2\tau_\eta/3$. Note how when the filter is not very large and with large spatial errors we have strong nonmonotonic behavior for the local slopes (DNS2b). (b) The effect of filter width on data from EXP2 experiment ($R_\lambda = 690$, small measurement volume). We tested four different filter widths: $\sigma/\tau_\eta = \frac{1}{6}, \frac{1}{3}, \frac{2}{3},$ and $\frac{4}{3}$.

$\sim \tau_\eta$ for increasing filter widths). A similar trend is observed in the experimental data [Fig. 8(b)]. In this case, choosing the filter width to be in the range $\tau \in \left[\frac{1}{6}, \frac{1}{3}\right]\tau_\eta$ seems to be optimal, minimizing the dependence on the filter width and the effects on the relevant time lags. Understanding filter effects may be even more important for experiments with particles much larger than the Kolmogorov scale. In those cases, the particle size naturally introduces a filtering by averaging velocity fluctuations over its size, i.e., those particles are not faithfully following the fluid trajectories.[11,15]

IV. CONCLUSION AND PERSPECTIVES

A detailed comparison between state-of-the-art experimental and numerical data of Lagrangian statistics in turbulent flows has been presented. The focus has been on single-particle Lagrangian structure functions. Only through the critical comparison of experimental and DNS data is it possible to achieve a quantitative understanding of the velocity scaling properties over the entire range of time scales and for a wide range of Reynolds numbers.

In particular, the availability of high Reynolds number experimental measurements allowed us to assess in a robust way the existence of very intense fluctuations, with high intermittency in the Lagrangian statistics around $\tau \in (2-6)\tau_\eta$. For larger time lags $\tau > 10\tau_\eta$, the signature of different statistics seems to emerge, with again good agreement between DNS and experiment (see Fig. 5). Whether the trend of logarithmic local slopes at larger times is becoming more and more extended at larger and larger Reynolds number is an issue for further research.

Both experiments and numerics show in the ESS local slope of the fourth- and sixth-order Lagrangian structure functions a dip region at around time lags $(2-6)\tau_\eta$ and a flattening at $\tau > 10\tau_\eta$. As of today, it is unclear whether the dip or the flattening region gives the asymptotic scaling properties of Lagrangian turbulence. The question of which region will extend as a function of Reynolds number cannot be resolved at present and remains open for future research.

It would also be important to probe the possible relations between Eulerian and Lagrangian statistics, as suggested by simple phenomenological multifractal models.[13,23,46,47] In these models, the translation between Eulerian (single-time) spatial statistics and Lagrangian statistics is made via the dimensional expression of the local eddy turnover time at scale r: $\tau_r \sim r/\delta_r u$. This allows predictions for Lagrangian statistics if the Eulerian counterpart is known. An interesting application concerns Lagrangian acceleration statistics,[18] where this procedure has given excellent agreement with experimental measurements. When applied to single-particle velocities, multifractal predictions for the LVSF scaling exponents are close to the plateau values observed in DNS at time lags $\tau > 10\tau_\eta$. It is not at all clear, however, if this formalism is able to capture the complex behavior of the local scaling exponents close to the dip region $\tau \in (2-6)\tau_\eta$, as depicted in Fig. 5. Indeed, multifractal phenomenology, as with all multiplicative random cascade models,[34] does not contain any signature of spatial structures such as vortex filaments. It is possible that in the Lagrangian framework, a more refined matching to the viscous dissipative scaling is needed, as proposed in Ref. 13, rephrasing known results for Eulerian statistics.[40] Even less clear is the relevance for Lagrangian turbulence of other phenomenological models based on superstatistics,[43] as recently questioned in Ref. 59.

The formulation of a stochastic model able to capture the whole shape of local scaling properties from the smallest to larger time lag, as depicted in Fig. 5, remains an open important theoretical challenge.

[1] S. B. Pope, "Lagrangian PDF methods for turbulent flows," Annu. Rev. Fluid Mech. **26**, 23 (1994).

[2] S. B. Pope, *Turbulent Flows* (Cambridge University Press, Cambridge, 2000).

[3] B. Sawford, "Turbulent relative dispersion," Annu. Rev. Fluid Mech. **33**, 289 (2001).

[4] P. K. Yeung, "Lagrangian investigations of turbulence," Annu. Rev. Fluid Mech. **34**, 115 (2002).

[5] P. K. Yeung and S. B. Pope, "Lagrangian statistics from direct numerical simulations of isotropic turbulence," J. Fluid Mech. **207**, 531 (1989).

[6] M. Virant and Th. Dracos, "3D PTV and its application on Lagrangian motion," Meas. Sci. Technol. **8**, 1539 (1997).

[7] G. A. Voth, K. Satyanarayan, and E. Bodenschatz, "Lagrangian acceleration measurements at large Reynolds numbers," Phys. Fluids **10**, 2268 (1998).

[8] S. Ott and J. Mann, "An experimental investigation of the relative diffusion of particle pairs in three-dimensional turbulent flow," J. Fluid Mech. **422**, 207 (2000).

[9] A. La Porta, G. A. Voth, A. M. Crawford, J. Alexander, and E. Bodenschatz, "Fluid particle accelerations in fully developed turbulence," Nature (London) **409**, 1017 (2001).

[10] N. Mordant, P. Metz, O. Michel, and J. F. Pinton, "Measurement of Lagrangian velocity in fully developed turbulence," Phys. Rev. Lett. **87**, 214501 (2001).

[11] G. A. Voth, A. La Porta, A. M. Crawford, J. Alexander, and E. Bodenschatz, "Measurement of particle accelerations in fully developed turbulence," J. Fluid Mech. **469**, 121 (2002).

[12] B. L. Sawford, P. K. Yeung, M. S. Borgas, P. Vedula, A. La Porta, A. M. Crawford, and E. Bodenschatz, "Conditional and unconditional acceleration statistics in turbulence," Phys. Fluids **15**, 3478 (2003).

[13] L. Chevillard, S. G. Roux, E. Lévêque, N. Mordant, J.-F. Pinton, and A. Arneodo, "Lagrangian velocity statistics in turbulent flows: Effects of dissipation," Phys. Rev. Lett. **91**, 214502 (2003).

[14] I. M. Mazzitelli, D. Lohse, and F. Toschi, "Effect of microbubbles on developed turbulence," Phys. Fluids **15**, L5 (2003).

[15] N. Mordant, E. Lévêque, and J.-F. Pinton, "Experimental and numerical study of the Lagrangian dynamics of high Reynolds turbulence," New J. Phys. **6**, 116 (2004).

[16] N. Mordant, A. M. Crawford, and E. Bodenschatz, "Experimental Lagrangian acceleration probability density function measurement," Physica D **193**, 245 (2004).

[17] I. M. Mazzitelli and D. Lohse, "Lagrangian statistics for fluid particles and bubbles in turbulence," New J. Phys. **6**, 203 (2004).

[18] L. Biferale, G. Boffetta, A. Celani, B. J. Devenish, A. Lanotte, and F. Toschi, "Multifractal statistics of Lagrangian velocity and acceleration in turbulence," Phys. Rev. Lett. **93**, 064502 (2004).

[19] P. K. Yeung, D. A. Donzis, and K. R. Sreenivasan, "High-Reynolds-number simulation of turbulent mixing," Phys. Fluids **17**, 081703 (2005).

[20] B. Lüthi, A. Tsinober, and W. Kinzelbach, "Lagrangian measurement of vorticity dynamics in turbulent flow," J. Fluid Mech. **528**, 87 (2005).

[21] L. Chevillard, S. G. Roux, E. Lévêque, N. Mordant, J.-F. Pinton, and A. Arneodo, "Intermittency of velocity time increments in turbulence," Phys. Rev. Lett. **95**, 064501 (2005).

[22] K. Hoyer, M. Holzner, B. Luthi, M. Guala, A. Liberzon, and W. Kinzelbach, "3D scanning particle tracking velocimetry," Exp. Fluids **39**, 923 (2005).

[23] L. Biferale, G. Boffetta, A. Celani, A. Lanotte, and F. Toschi, "Particle trapping in three dimensional fully developed turbulence," Phys. Fluids **17**, 021701 (2005).

[24] N. T. Ouellette, H. Xu, M. Bourgoin, and E. Bodenschatz, "Small-scale anisotropy in Lagrangian turbulence," New J. Phys. **8**, 102 (2006).

[25] J. Bec, L. Biferale, G. Boffetta, A. Celani, M. Cencini, A. Lanotte, S. Musacchio, and F. Toschi, "Acceleration statistics of heavy particles in turbulence," J. Fluid Mech. **550**, 349 (2006).

[26] H. Xu, M. Bourgoin, N. T. Ouellette, and E. Bodenschatz, "High order Lagrangian velocity statistics in turbulence," Phys. Rev. Lett. **96**, 024503 (2006).

[27] P. K. Yeung, S. B. Pope, and B. L. Sawford, "Reynolds number dependence of Lagrangian statistics in large numerical simulations of isotropic turbulence," J. Turbul. **7**, 58 (2006).

[28] N. T. Ouellette, H. Xu, M. Bourgoin, and E. Bodenschatz, "An experimental study of turbulent relative dispersion models," New J. Phys. **8**, 109 (2006).

[29] J. Bec, L. Biferale, M. Cencini, A. Lanotte, and F. Toschi, "Effects of vortex filaments on the velocity of tracers and heavy particle in turbulence," Phys. Fluids **18**, 081702 (2006).

[30] M. Guala, A. Liberzon, A. Tsinober, and W. Kinzelbach, "An experimental investigation on Lagrangian correlations of small-scale turbulence at low Reynolds number," J. Fluid Mech. **574**, 405 (2007).

[31] S. Ayyalasomayajula, A. Gylfason, L. R. Collins, E. Bodenschatz, and Z. Warhaft, "Lagrangian measurements of inertial particle accelerations in grid generated wind tunnel turbulence," Phys. Rev. Lett. **97**, 144507 (2007).

[32] P. K. Yeung, S. B. Pope, E. A. Kurth, and A. G. Lamorgese, "Lagrangian conditional statistics, acceleration and local relative motion in numerically simulated isotropic turbulence," J. Fluid Mech. **582**, 399 (2007).

[33] H. Homann, R. Grauer, A. Busse, and W. C. Müller, "Lagrangian statistics of Navier-Stokes- and MHD-turbulence," J. Plasma Phys. **73**, 821 (2007).

[34] U. Frisch, *Turbulence: The legacy of A. N. Kolmogorov* (Cambridge University Press, Cambridge, 1995).

[35] R. Benzi, G. Paladin, G. Parisi, and A. Vulpiani, "On the multifractal nature of fully developed turbulence and chaotic systems," J. Phys. A **17**, 3521 (1984).

[36] Z. S. She and E. Lévêque, "Universal scaling laws in fully developed turbulence," Phys. Rev. Lett. **72**, 336 (1994).

[37] B. Castaing, Y. Gagne, and E. J. Hopfinger, "Velocity probability density functions of high Reynolds number turbulence," Physica D **46**, 435 (1990).

[38] V. Yakhot, "Mean-field approximation and a small parameter in turbulence theory," Phys. Rev. E **63**, 026307 (2001).

[39] R. Benzi, L. Biferale, G. Paladin, A. Vulpiani, and M. Vergassola, "Multifractality in the statistics of the velocity gradients in turbulence," Phys. Rev. Lett. **67**, 2299 (1991).

[40] U. Frisch and M. Vergassola, "A prediction of the multifractal model—The intermediate dissipation range," Europhys. Lett. **14**, 439 (1991).

[41] A. Arneodo, C. Baudet, F. Belin, R. Benzi, B. Castaing, B. Chabaud, R. Chavarria, S. Ciliberto, R. Camussi, F. Chillà, B. Dubrulle, Y. Gagne, B. Hebral, J. Herweijer, M. Marchand, J. Maurer, J. F. Muzy, A. Naert, A. Noullez, J. Peinke, F. Roux, P. Tabeling, W. van de Water, and H. Willaime, "Structure functions in turbulence, in various flow configurations, at Reynolds number between 30 and 5000, using extended self-similarity," Europhys. Lett. **34**, 411 (1996).

[42] F. G. Schmitt, "Relating Lagrangian passive scalar scaling exponents to Eulerian scaling exponents in turbulence," Physica A **48**, 129 (2005).

[43] C. Beck, "Statistics of three-dimensional Lagrangian turbulence," Phys. Rev. Lett. **98**, 064502 (2007).

[44] A. S. Monin and A. M. Yaglom, *Statistical Fluid Mechanics* (MIT, Cambridge, MA, 1975), Vol. II.

[45] R.-C. Lien and E. A. Dásaro, "The Kolmogorov constant for the Lagrangian spectrum and structure function," Phys. Fluids **14**, 4456 (2002).

[46] M. S. Borgas, "The multifractal Lagrangian nature of turbulence," Philos. Trans. R. Soc. London, Ser. A **342**, 379 (1993).

[47] G. Boffetta, F. De Lillo, and S. Musacchio, "Lagrangian statistics and temporal intermittency in a shell model of turbulence," Phys. Rev. E **66**, 066307 (2002).

[48] N. T. Ouellette, H. Xu, and E. Bodenschatz, "A quantitative study of three-dimensional Lagrangian particle tracking algorithms," Exp. Fluids **40**, 301 (2006).

[49] T. Gotoh, D. Fukayama, and T. Nakano, "Velocity field statistics in homogeneous steady turbulence obtained using a high-resolution direct numerical simulation," Phys. Fluids **14**, 1065 (2002).

[50] Y. Kaneda, T. Ishihara, M. Yokokawa, K. Itakura, and A. Uno, "Energy dissipation rate and energy spectrum in high resolution direct numerical simulations of turbulence in a periodic box," Phys. Fluids **15**, L21 (2003).

[51] S. Chen, G. D. Doolen, R. H. Kraichnan, and Z.-S. She, "On statistical correlations between velocity increments and locally averaged dissipation in homogeneous turbulence," Phys. Fluids A **5**, 458 (1993).

[52]H. Homann, J. Dreher, and R. Grauer, "Impact of the floating-point precision and interpolation scheme on the results of DNS of turbulence by pseudo-spectral codes," Comput. Phys. Commun. **117**, 560 (2007).

[53]V. Yakhot and K. R. Sreenivasan, "Anomalous scaling of structure functions and dynamic constraints on turbulence simulations," J. Stat. Phys. **121**, 823 (2005).

[54]We notice that in DNS, the integral scale is defined as $L \equiv \pi$ and is well approximated by the value $L \sim v'^3_{\mathrm{rms}}/\epsilon$ used for dimensional arguments.

[55]The error bars in this and the following figures have been computed as the statistical spread among the LVSF of the three components. We warn the reader about the fact that, in principle, the error bars so defined depend on the choice of the coordinate system orientation [with the exception of $S_2(\tau)$].

[56]L. Biferale and I. Procaccia, "Anisotropy in turbulent flows and in turbulent transport," Phys. Rep. **414**, 43 (2005).

[57]R. Benzi, S. Ciliberto, R. Tripiccione, C. Baudet, F. Massaioli, and S. Succi, "Extended self-similarity in turbulent flows," Phys. Rev. E **48**, R29 (1993).

[58]J. Berg Jorgensen, J. Mann, S. Ott, H. L. Pécseli, and J. Trulsen, "Experimental studies of occupation and transit times in turbulent flows," Phys. Fluids **17**, 035111 (2005).

[59]T. Gotoh and R. H. Kraichnan, "Turbulence and Tsallis statistics," Physica D **193**, 231 (2004).

[60]iCFDdatabase (http://cfd.cineca.it).